Development of energy-saving devices for a full slow-speed ship through improving propulsion performance

Jung-Hun Kim[1], Jung-Eun Choi[2], Bong-Jun Choi[1], Seok-Ho Chung[1] and Heung-Won Seo[1]

[1]Hyundai Heavy Industries Co., LTD, Ulsan, Korea
[2]Global Core Research Center for Ships and Offshore Plants, Pusan National University, Busan, Korea

ABSTRACT: *Energy-saving devices for 317K VLCC have been developed from a propulsion standpoint. Two ESD candidates were designed via computational tools. The first device WAFon composes of flow-control fins adapted for the ship wake to reduce the loss of rotational energy. The other is WAFon-D, which is a WAFon with a duct to obtain additional thrust and to distribute the inflow velocity on the propeller plane uniform. After selecting the candidates from the computed results, the speed performances were validated with model-tests. The hydrodynamic characteristics of the ESDs may be found in improved hull and propulsive efficiencies through increased wake fraction.*

KEY WORDS: Energy-saving device; VLCC; CFD; Model test; Duct; Flow-control fin; Propulsion performance.

INTRODUCTION

Shipbuilding will continue to be reorganized to an industry driven by eco-friendliness, which signifies that developing core technologies to cut greenhouse gas emission of ships will be increasingly essential. Climbing oil prices also raise the necessity to develop Energy-Saving Devices (ESDs). These devices minimize the energy loss during sail or partially recover the lost energy. The energy loss during sail on calm water may be due to ① resistance from wave-making, viscous, and wind; ② propulsion including the momentum loss from the accelerated flow velocity while passing the propeller, energy loss from the rotational flow of the propeller slipstream, and viscous loss from the hull-form and frictional force; and ③ loss from exhaust gas and heat. Part of the lost energy is recovered by the propeller and the rudder. Another means to conserve is taking advantage of an ESD. The device does have a downside of additional costs arising from the complexity in the hull structure. The increase in fuel costs and international environment regulations, however, have outweighed this point, leading to the development of various ESDs that reduce fuel consumption through more improved performance in the ship's resistance and propulsion.

Various types of ESDs have been developed since the energy crisis in the late 1970s. The ESDs may be categorized into three groups. One is located in front of propeller improving the inflow on the propeller plane. Another utilizes the rotational flow of the propeller slipstream. The other is composite ESD that incorporates the merits of both types. This study aims to develop an ESD suited for a full slow-speed ship. In the case of a full slow-speed ship, a pair of strong vortices occurs transfering from the parallel middle body to the stern due to the sudden changes in the aft body, and flows into the propeller plane. This is a factor that undermines the ship's resistance, propulsion and cavitation performances by creating non-uniformity of propeller inflow. Various types of ESDs are being developed to dispel such drops in performance. The vortex generator is an ESD that

---

enhances the propeller's cavitation performance through uniform velocity distribution in propeller inflows by using the tip vortex to move the large momentum from outer to inner parts of the boundary layer (Lee et al., 2004; Choi et al., 2009). The low viscous fin (Masuko et al., 1998) is another type of ESD that weakens the bilge vortices to improve the velocity distribution of the propeller inflow and reduce the viscous resistance resulting from the pressure recovery in the stern. A Pre-Swirl Stator (PSS) that increases propulsive efficiency by decreasing the propeller slipstream's swirl energy via generating or improving the rotational flow in advance has also been devised (Lee et al., 1992; Lee et al., 1994; Kim et al., 1993; Yang et al., 2000; 2001; Kang et al., 2004). Reaction fins work with the similar energy-saving mechanism of PSS (Kawakita et al., 2012). Another type of ESD installs a duct that uniformizes the velocity distribution on the propeller plane and generates additional thrust on the foil section (Schneekluth, 1986). There is also an ESD that utilizes the hydrodynamic traits of the PSS and duct (Mewis and Guiard, 2011; Dang, 2012; Shin et al., 2013). CFD becomes a powerful tool for the design of ESD due to the rapid development of numerical method and computer power. Morgut and Nobile (2012) compared the flow characteristics around propellers in uniform inflow utilizing two different mesh types, i.e., hexa-structured and hybrid-unstructured meshes. They showed that the hybrid-unstructured meshes seemed to exhibit a more diffusive characteristics character than the hexa-structured meshes, although these meshes guarantee similar levels of accuracy. The hybrid mesh system is applied to predict flow characteristics around a propeller operating behind a ship. Seo et al. (2010) utilized unstructured meshes in the bow and stern region, and structured meshes in the rest of the domain. Park et al. (2013) developed SNUFORM code using open source libraries to predict the performance of ship resistance. Ji et al. (2011; 2012) simulated the cavitating flows around a propeller in both uniform and wake flow. Paik et al. (2014) simulated cavitation flow and hull pressure fluctuation for a propeller operating behind a hull using a commercial code of Fluent.

In this study, ESDs that improve the propulsion performance of a full slow-speed ship 317k VLCC have been designed using CFD and validated with model tests. The second chapter of the paper will look into objective ship and computational conditions; the third of effective CFD technologies to develop ESD; the fourth will deal with the design concept of the device; the fifth of the development of ESD using CFD; and the sixth and seventh of model-ship performance analysis method and evaluation of ESD with towing-tank experiments.

OBJECTIVE SHIP AND COMPUTATIONAL CONDITIONS

The principal dimensions of the objective ship and propeller are laid out in Table 1.

Table 1 Principal dimensions of a ship and a propeller.

Length between perpendicular (LPP)	319.0 m
Breadth (B)	60.0 m
Draft (T)	21.0 m
Propeller diameter (D_P)	10.0 m
No. of propeller blade (Z)	4

The model-ship scale ratio is 45.00, and F_N=0.141, R_{NM}=7.305×10^6 at ship design speed (V_S). F_N and R_N are non-dimensional values of V_S and LPP. And the subscript M and S refer to the model and ship scale, respectively.

EFFECTIVE CFD TECHNOLOGIES

This study does not go into what the computational method is. The details and the formulations of the numerical methodologies for CFD are well known and extensively documented in many literatures. Hence, only the main features of the methodologies will be described in this paper. The details may be found in Choi et al. (2010).

The governing equations are the continuity and the Navier-Stokes equations of unsteady turbulent flow. These equations are expressed in tensor notation as follows:

$$\frac{\partial U_i}{\partial x_i} = 0 \tag{1}$$

$$\rho \frac{\partial U_i}{\partial t} + \rho U_\ell \frac{\partial U_i}{\partial x_\ell} = -\frac{\partial p}{\partial x_i} + \frac{\partial}{\partial x_\ell}\left(\mu \frac{\partial U_i}{\partial x_\ell} - \rho \overline{u_i u_\ell}\right) \tag{2}$$

where $U_i = (U, V, W)$ is the velocity component in $x_i = (x, y, z)$ direction, while p, ρ, μ and $-\rho \overline{u_i u_\ell}$ are the static pressure, fluid density, fluid viscosity, and Reynolds stresses, respectively.

The turbulence model applied is the Reynolds stress model. The free surface was treated as a double-body model. The Reynolds stress turbulence model is applied for the turbulence closure since this model is superior to the others for the prediction of bilge vortices (Hino, 2005). The computations are carried out at towing and self-propulsion conditions with the ESD attached. The sliding-mesh method was employed to simulate the flow around operating propeller. Fluent v.13 was utilized.

An efficient CFD technology has been developed to save the computational time required to analyze the flow around the model ship equipped with propeller, rudder, and ESD. A hybrid grid system that incorporates both structured and unstructured grids was used as seen in Fig. 1. The grids were generated using Pointwise for structured grids and Hypermesh for the unstructured grids. To verify the computational results using the hybrid grid system, the structured grid system were used at the towing condition of the bare hull.

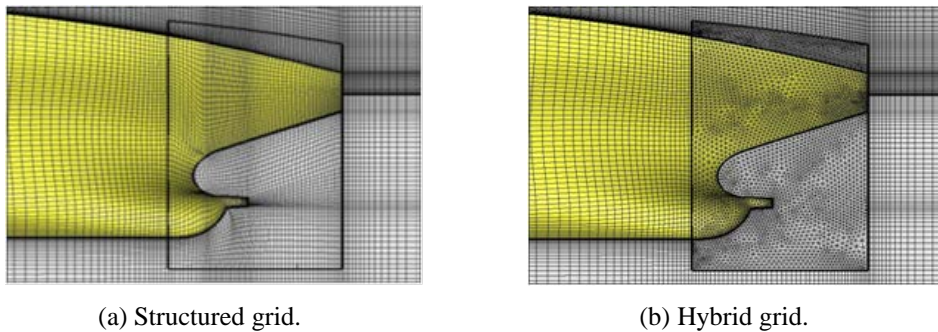(a) Structured grid.   (b) Hybrid grid.

Fig. 1 View of grid types.

Fig. 2 shows the axial velocity contour and velocity vector on the propeller plane. The velocity components are non-dimensionalized by the model ship speed. The wake fractions are 0.450 and 0.462 for the structured and hybrid grid systems, respectively. The marginal error between structured and hybrid grid systems is around 3%.

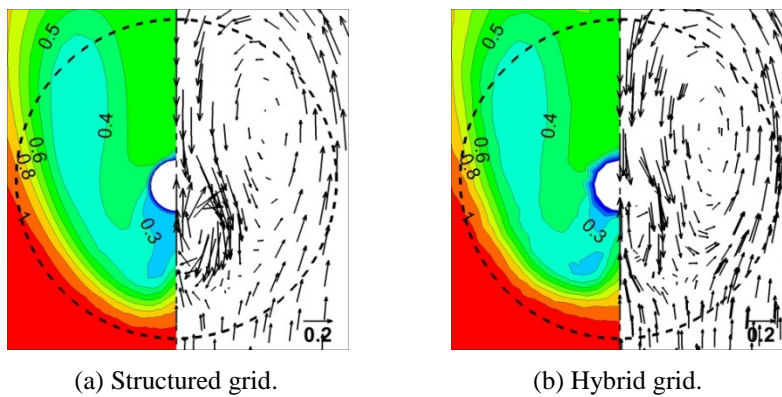(a) Structured grid.   (b) Hybrid grid.

Fig. 2 Axial velocity contour and velocity vector on the propeller
plane using structured and hybrid grid systems.

A partial computational domain was used to save computational time. Analysis of the interpretation drawn by altering the inlet boundary plane revealed that St. 10 was the optimal inlet boundary plane. The computational domain is from midship to 1.5 LPP in x-direction, and 1.0 LPP in y- and z-direction. The number of grids is 1,537,762 with 651,988 of hexahedral and 555,862 of tetrahedral type around a hull, and 329,913 of tetra type around a propeller. The average space of the first grid from the hull and the propeller is $y^+=80$ in wall coordinate. The values of inlet boundary plane were drawn from those of the full computational domain. Fig. 3 depicts the grids and inlet boundary plane used to calculate the flow at self-propulsion condition considering the propeller geometry by tapping into the partial domain and sliding-mesh methodology.
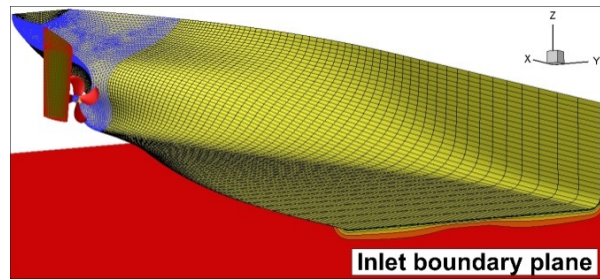

Fig. 3 View of grid generation and inlet boundary plane.

Fig. 4 depicts the time history between the propeller thrust and the resistance on the hull. The time interval was 1° rotation, relaxation factor was 0.2, and a sub-iteration number of 45 were employed. The convergence is obtained after 1 second. The number of grid cells is 3 million.
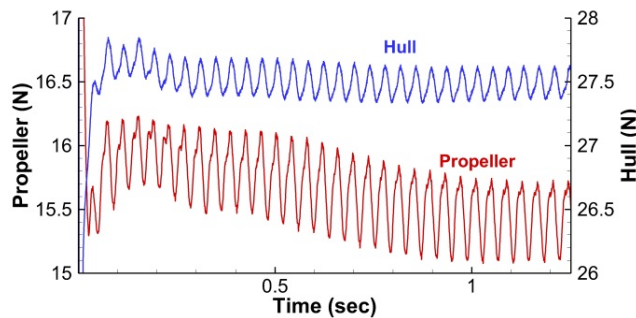

Fig. 4 Time history of propeller thrust and viscous resistance of hull under self-propulsion calculation.

Fig. 5 shows the axial velocity contour of the propeller slipstream using the full and partial domains. The wake fractions are 0.096680 and 0.097703 for the full and partial domains, respectively. The marginal error between the partial and full computations is around 1%.
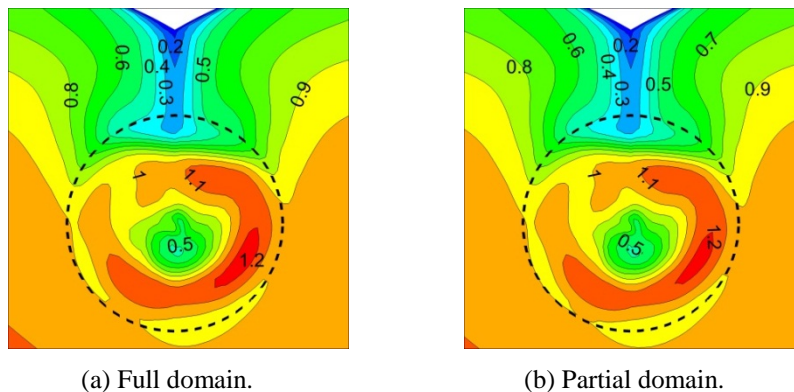
       (a) Full domain.   (b) Partial domain.

Fig. 5 Axial velocity contour and velocity vector on the propeller plane using structured and hybrid grid systems.

394

Int. J. Nav. Archit. Ocean Eng. (2015) 7:390~398

The calculation was done by a 60 core (2.67 *GHz* Xeon processors) Linux Cluster. Employing a hybrid grid and partial computation domain cut the duration of computing the self-propulsion condition from two and half to one day.

DESIGN CONCEPT OF ESD

The objective of the ESD study is to circumvent the existing patents on the devices and develop an ESD with stellar propulsive performance. To this aim, the inflow velocity distribution on the propeller plane in a bare hull condition needs to be studied beforehand as seen in Fig. 2. There exists large bilge vortices and low speed area on the upper propeller plane of the objective ship. In such case, an ESD that enhances the wake is effective, as energy is lost due to the friction from the relatively large expanded area ratio of propeller.

This study aims to develop a device to recollect part of the energy lost from the accelerated momentum passing the propeller and the loss of swirl energy from propeller slipstream while sailing on calm water. One approach is to install a duct on the propeller front to ensure uniformity of the velocity distribution on the propeller plane. The duct also serves to reduce the resistance of the ship by creating additional thrust sourced from the converged duct and foil effect as may be seen in Fig. 6.
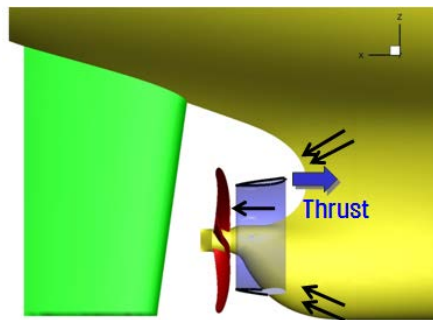

Fig. 6 Sketch of duct effect.

Fig. 7 depicts the velocity vector on the front and back of the propeller. As a means to reduce the loss of swirl energy of the propeller slipstream as shown in Fig. 7(b), a flow-control fin (or a stator) which is an ESD that creates rotational flow in the opposite direction from the propeller inflow may be attached.

(a) Ahead propeller.　　　　　　　　　　(b) After propeller.

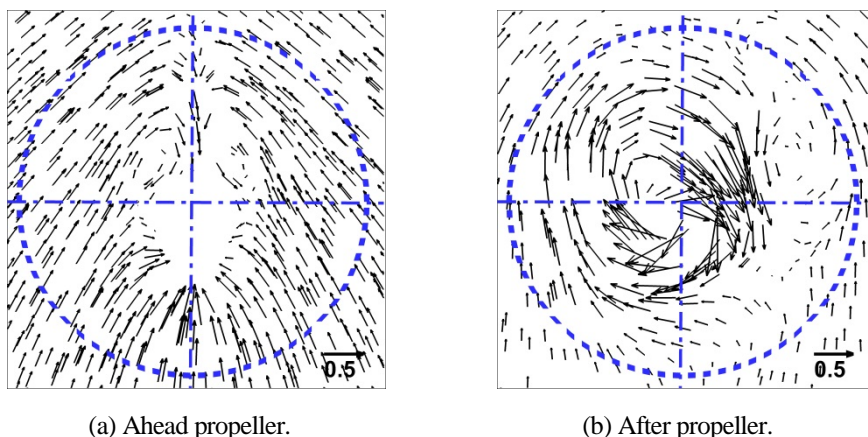Fig. 7 Velocity vector on the plane of ahead and after propeller.

The duct and fin, which are shaped like a hydrofoil, are closely related to the wake distribution and there exists an optimal angle of attack (or α). The fin has been designed so that the α is constant. This has been named the WAFon (wake adapted flow control fin) and the WAFon with ducts has been named the WAFon-D, as are depicted in Fig. 8.
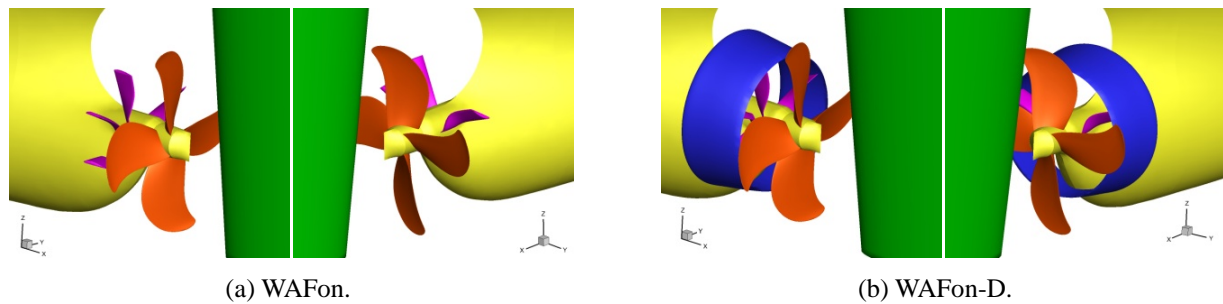
(a) WAFon.   (b) WAFon-D.

Fig. 8 Views of WAFon and WAFon-D.

The optimal α of the flow-control fin with high propulsive performance was obtained on the minimal viscous resistance under self-propulsion condition ($R_{VM}{}^{SP}$) and delivered power ($PD_M=2\pi\cdot n_M\cdot Q_M$, where Q is propeller torque) with CFD, and have been verified in model tests. The superscript SP stands for the self-propulsion condition.

ESD DESIGN USING CFD

The self-propulsion point was obtained from the load-varying tests that employ the results from two propeller rotating speeds (Choi et al., 2010). The parametric studies of duct (diameter, position, phase angle) and flow-control fin (length, position, pitch angle) were carried out using CFD. The rate of viscous resistance ($\Delta R_{VM}{}^{SP}$), propeller rotating speed (Δn_M), and delivered power (ΔPD_M) at the self-propulsion point are indicated in Table 2. The rate refers to the value as compared with the results from the bare hull without ESD.

Table 2 Rates of viscous resistance, propeller rotative speed and delivered power of WAFon and WAFon-D.

	$\Delta R_{VM}{}^{SP}$ (*N*)	Δn_M (%)	ΔP_{DM} (%)
WAFon	-0.2204	-2.8	-2.5
WAFon-D	-0.3821	-5.0	-3.6

MODEL-SHIP PERFORMANCE ANALYSIS METHOD

The speed performance of the ship was estimated using the ITTC-78 model-ship performance method. ITTC-78's full scale wake (w_{TS}) expansion method divides the model scale wake (w_{TM}) with the potential ($w_{TM}{}^P$) and viscous components ($w_{TM}{}^V$) as expressed in Eqs. (3) ~ (5), which means there is no scale effect of $w_{TM}{}^P$. The scale effect of $w_{TM}{}^V$ adopts the Sasajima method that reduces by the ratio of the viscous resistance coefficient of the ship and model. Note that the magnitude of $w_{TS}{}^P$ is equal to that of thrust deduction fraction (t) in the potential flow. The value of 0.04 was proposed to take into account the rudder effect. $\triangle C_F$ is the model-ship correlation allowance.

$$w_{TS} = w_{TM}{}^P + w_{TM}{}^V (C_{VS} + \Delta C_F) / C_{VM} \tag{3}$$

$$w_{TM}{}^P = t + 0.04 \tag{4}$$

$$w_{TM}{}^V = w_{TM} - w_{TM}{}^P \tag{5}$$

The modified ITTC-78 (Hereinafter referred to as 'M. ITTC-78') calculates the w_{TS} by the same equation as (3). The wake variance due to the ESD ($w_{TM}-w_{TM}{}^{w/oESD}$) is assumed as $w_{TM}{}^P$ as in Eq. (6), and the remainder as $w_{TM}{}^V$ as in (7).

$$w_{TM}{}^{P} = t + 0.04 + (w_{TM} - w_{TM}{}^{w/oESD}) \tag{6}$$

$$w_{TM} = w_{TM} - w_{TM}{}^{P} \tag{7}$$

The ITTC-99 model-ship performance method's ship scale wake expansion method (Hereinafter 'ITTC-99') is limited to PSS. The entirety of the wake variation due to the ESD is assumed to be $w_{TM}{}^{P}$, and the $w_{TM}{}^{V}$ arising from the ESD is not taken into consideration as expressed in Eqs. (6) and (8).

$$w_{TM}{}^{V} = w_{TM}{}^{V(w/oESD)} \tag{8}$$

The direct method (Hereinafter referred to as 'Direct') does not calculate w_{TS} using the interpretation of ITTC-78 in (3), but takes a direct route by neglecting the scale effect from the ESD as seen in (9).

$$w_{TS} = 1 - \left(\frac{1 - w_{Ts}}{1 - w_{TM}} \right)^{w/oESD} \cdot (1 - w_{TM}) \tag{9}$$

EVALUATION OF ESD WITH MODEL TESTS

The model tests to estimate the speed performance with the WAFon and WAFon-D, and those without the ESD were carried out in the towing tank of Hyundai Heavy Industries (HHI). Table 3 displays the results of the self-propulsion tests. Both the WAFon and WAFon-D serve to lesson n_M. However, the WAFon increases Q_M, whereas the WAFon-D decreases Q_M. As a result, the delivered powers of WAFon and WAFon-D in model scale are reduced by 0.4% and 5.4%, respectively.

Table 3 Experimental data of self-propulsion tests.

ESD	n_M (*rps*)	T_M (*N*)	Q_M (*N·m*)	PD_M (*W*)	ΔPD_M (%)
Without	7.89	26.67	0.6708	33.3	0.0%
WAFon	7.81	27.39	0.6751	33.1	-0.4%
WAFon-D	7.65	27.10	0.6543	31.5	-5.4%

The performance was evaluated using the three methods of ship scale wake expansion noted in the previous chapter. Table 4 relays the self-propulsion factors and the speed performances for the WAFon.

Table 4 Self-propulsion factors and speed performances of a ship with WAFon using four full-scale wake expansion methods.

Analysis method	t	w_{TM}	w_{TS}	η_H	η_R	η_O	η_D	PD (*kW*)	ΔPD (%)	ΔV_S (kts)	Δn_S (%)
Without	0.235	0.432	0.353	1.183	1.010	0.594	0.706	22,971	0.0	16.21	0.0
ITTC-78	0.253	0.473	0.379	1.203	1.022	0.581	0.712	22,785	-0.8	0.04	-0.5
ITTC-99	0.253	0.473	0.395	1.234	1.022	0.575	0.724	22,394	-2.5	0.13	-1.4
M. ITTC-78	0.253	0.473	0.400	1.246	1.022	0.572	0.728	22,274	-3.0	0.16	-1.8
Direct	0.253	0.473	0.400	1.246	1.022	0.572	0.728	22,273	-3.0	0.16	-1.8

WAFon serves to enhance both t and w_{TS} but the rate is greater with w_{TS}, so the hull efficiency (η_H) increases. The relative rotative efficiency (η_R) is not so much changed. The propeller open water efficiency (η_O) decreases due to the increased w_{TS}, but its magnitude is less than that of increased η_H. In conclusion, WAFon enhances the propulsive efficiency (η_D) higher with increased η_H, and the speed performance higher with lower PD. Accordingly, WAFon enhances the speed by 0.16 knots due to the effect of reducing PD by 3.0% in a condition with n_S 1.4 rpm lower (-1.8%). All the four full-scale wake expansion methods show similar trend, however, the w_{TS} of the M. ITTC-78 and direct methods are the highest. The rise in w_{TS} (or the fall in V_A, where V_A is propeller advance velocity) serves to increase α. It should be noted that the fins need to take propeller cavitation into consideration.

Table 5 indicates the self-propulsion factors and the speed performances for the WAFon-D. With regard to WAFon-D, the trend is similar to that of WAFon, but the increase in t is relatively smaller and that of w_{TS} is greater, furthering raising η_H to enhance η_D as well. Therefore, the PD is further reduced to enhance speed performance. The speed increased 0.32 *knots* accordingly, as the PD was reduced by 6.1% leading the n_S to lessen 2.13 *rpm* (-2.6%).

Table 5 Self-propulsion factors and speed performances of a ship with WAFon-D using four full-scale wake expansion methods.

Analysis method	t	w_{TM}	w_{TS}	η_H	η_R	η_O	η_D	PD (*kW*)	ΔPD (%)	ΔV_S (kts)	Δn_S (%)
Without	0.235	0.432	0.353	1.183	1.010	0.594	0.706	22,971	0.0	16.21	0.0
ITTC-78	0.249	0.502	0.390	1.232	1.034	0.576	0.734	22,232	-3.2	0.17	-1.4
ITTC-99	0.249	0.502	0.423	1.302	1.034	0.561	0.754	21,637	-5.8	0.31	-2.5
M. ITTC-78	0.249	0.502	0.433	1.324	1.034	0.557	0.759	21,475	-6.5	0.34	-3.0
Direct	0.249	0.502	0.427	1.311	1.034	0.559	0.756	21,574	-6.1	0.32	-2.6

CONCLUSION

Energy-saving devices WAFon and WAFon-D that serve to enhance the propeller inflow and reduce the loss of swirl energy in the slipstream have been designed utilizing CFD and verified with model tests. The ESDs were designed with a consideration of the hull wake. The hydrodynamic properties of the ESD lie in the greater hull efficiency tapping into the rise in effective wake fraction, and hull and propulsive efficiencies. The delivered powers of WAFon and WAFon-D have been reduced by 3.0% and 6.1%, respectively. To install these stellar ESDs to a ship, the simpler shape is to be studied further taking productivity into consideration. The research will contribute to strengthening competitiveness in gaining orders by cutting daily fuel oil consumption; increasing sales based on higher performance; and better responding to international environmental regulations by curtailing exhaust gas emissions.

ACKNOWLEDGEMENTS

REFERENCES

Choi, J.E., Kim, J.H., Choi, B.J. and Lee, S.B., 2009. Computational prediction of speed performance for a ship with vortex generators. *Journal of the Society of Naval Architects of Korea*, 46(2), pp.136-147.

Choi, J.E., Min, K.S., Kim, J.H., Lee, S.B. and Seo, H.W., 2010. Resistance and propulsion characteristics of various commercial ships based on CFD results. *Ocean Engineering*, 37(7), pp.549-566.

Dang, J., 2012. An exploratory study on the working principles of energy saving devices (ESDs) – PIV, CFD investigations and ESD design guidelines. *Proceedings of the 31st International Conference on Ocean, Offshore and Arctic Engineering, OMAE2012-83053*, Rio de Janeiro, Brazil, 1-6 July 2012.

Hino, T. (Ed.), 2005. *Proceedings of CFD Workshop 2005*, Tokyo, Japan, 9-11 March 2005.

Ji, B., Luo, X., Peng, X., Wu, Y. and Xu, H., 2012. Numerical analysis of cavitation evolution and excited pressure fluctuation around a propeller in non-uniform wake. *International Journal of Multiphase Flow*, 43, pp.13-21.

Ji, B., Luo, X., Wang, X., Peng, X., Wu, Y. and Xu, H., 2011. Unsteady numerical simulation of cavitating turbulent flow around a fighly skewed model marine propeller. *Journal of Fluids Engineering-Transactions of the ASME*, 133(1), pp. 011102.

Masuko, A., Koshiba, Y. and Ishiguro, T., 1998. Energy Saving Device for Ships IHI - L.V. Fin. *Ishikawajima-Harima Engineering Review*, 38(6), pp.392-397.

Kang, Y.D., Kim, M.C. and Chun, H.H., 2004. A study on the design of a biased asymmetric pre-swirl stator propulsion system. *Journal of the Society of Naval Architects of Korea*, 41(3), pp.13-21.

Kawakita, C., Takashima, R. and Sato, K., 2012. CFD on cavitation around marine propellers with energy-saving devices. *Mitsubishi Heavy Industries Technical Review*, 49(1), pp.63-67.

Kim, M.C., Lee, J.T., Suh, J.C. and Kim, H.C., 1993. A study on the asymmetric preswirl stator system. *Journal of the Society of Naval Architects of Korea*, 30(1), pp.30-44.

Lee, C.J., Park, I.R., Lee, Y.H. and Byeon, S.H., 2004. A study on the performances affected by vortex generator for DWT 40,000 ton product carrier. *Proceedings of the Annual Meeting, SNAK*, Sanchung, 20-22 October 2004, pp.257-263.

Lee, J.T., Kim, M.C., Suh, J.C., Kim, S.H. and Choi, J.G., 1992. Development of a preswirl stator-propeller system for improvement propulsion efficiency : a symmetric stator propulsion system. *Journal of the Society of Naval Architects of Korea*, 29(4), pp.132-145.

Lee, J.T., Kim, M.C., Van, S.H., Kim, K.S. and Kim, H.C., 1994. Development of a preswirl stator propulsion system for a 300K VLCC. *Journal of the Society of Naval Architects of Korea*, 31(1), pp.1-13.

Mewis, F., and Guiard, T., 2011. Mewis duct – new developments, solutions and conclusions. *Second International Symposium on Marine Propulsors*, Hamburg, Germany, June 2011.

Morgut, M. and Nobile, E., 2012. Influence of grid type and turbulence model on the numerical prediction of the flow around marine propellers working in uniform inflow. *Ocean Engineering*, 42, pp.26-34.

Paik, K.J., Park, H.G. and Seo, J.S., 2014. RANS simulation of cavitation and hull pressure fluctuation for marine propeller operating behind-hull condition. *International Journal of Naval Architecture and Ocean Engineering*, 5(4), pp.502-512.

Park, S.H., Park, S.W., Rhee, S.H., Lee, S.B., Choi, J.E. and Kang, S.H., 2013. Investigation on the wall function implementation for the prediction of ship resistance. *International Journal of Naval Architecture and Ocean Engineering*, 5(1), pp.33-46.

Schneekluth, H., 1986. Wake equalizing duct. *The Naval Architect*, 103, pp.147-150.

Seo, J.H., Seol, D.M., Lee, J.H. and Rhee, S.H., 2010. Flexible CFD meshing strategy for prediction of ship resistance and propulsion performance. *International Journal of Naval Architecture and Ocean Engineering*, 2(3), pp.139-145.

Shin, H.J., Lee, J.S., Lee, K.H., Han, M.R., Hur, E.B. and Shin, S.C., 2013. Numerical and experimental investigation of conventional and un-conventional preswirl duct for VLCC. *International Journal of Naval Architecture and Ocean Engineering*, 5(3), pp.414-430.

Yang, J.M., Lee, S.J., Kim, H.C., Suh, J.C. and Park, Y.M., 2000. Effect of pre-swirl stator vane on the pro-peller hull interaction of a full ship. *Proc. of the Annual Autumn Meeting, SNAK*, Ulsan, 9-10 November 2000, pp.188-191.

Yang, J.M., Kim, K., Park, K.H., Kim, H.C., Suh, J.C. and Park, Y.M., 2001. Effect of Pre-Swirl Stator Vane on the Propeller Hull Interaction (2). *Proceedings of the Annual Autumn Meeting, SNAK,* Seoul, 8-9 November 2001, pp.216-219.